Ultrasonics 56 (2015) 21–35

Contents lists available at ScienceDirect

Ultrasonics

journal homepage: www.elsevier.com/locate/ultras

Physical mechanisms of coherent acoustic phonons generation by ultrafast laser action

Pascal Ruello [a,*], Vitalyi E. Gusev [b]

[a] Institut des Molécules et Matériaux du Mans, UMR CNRS 6283, Université du Maine, 72085 Le Mans, France
[b] Laboratoire d'Acoustique UMR CNRS 6613, Université du Maine, 72085 Le Mans, France

ARTICLE INFO

Article history:
Received 15 December 2013
Received in revised form 26 May 2014
Accepted 3 June 2014
Available online 24 June 2014

Keywords:
Ultrafast phenomena
Ultrafast acoustics
Laser ultrasonics
Electron–phonon coupling
Nanoacoustics

ABSTRACT

In this review we address the microscopic mechanisms that are involved in the photogeneration processes of GHz–THz coherent acoustic phonons (CAP) induced by an ultrafast laser pulse. Understanding and describing the underlying physics is necessary indeed for improving the future sources of coherent acoustic phonons useful for the non-destructive testing optoacoustic techniques. Getting more physical insights on these processes also opens new perspectives for the emerging field of the opto-mechanics where lattice motions (surface and/or interfaces ultrafast displacements, nanostructures resonances) are controlled by light. We will then remind the basics of electron–phonon and photon-phonon couplings by discussing the deformation potential mechanism, the thermoelasticity, the inverse piezoelectric effect and the electrostriction in condensed matter. Metals, semiconductors and oxide materials will be discussed. The contribution of all these mechanisms in the photogeneration process of sound will be illustrated over several examples coming from the rich literature.

1. Introduction

Ultrafast light-induced coherent acoustic phonons in solids have been a subject of numerous studies since the end of the eighties thanks to the development of femtosecond laser sources. Most of the experiments were performed according to the all-optical pump–probe scheme where a femtosecond pulse (pump) excites a solid and leads, through different electron–phonon and photon-phonon coupling mechanisms, to the emission of GHz–THz coherent acoustic phonons (CAP). The probe laser beam, delayed in time, allows to detect them with time resolution of hundreds of femtoseconds. Pioneering experiments have been conducted with semiconductors and metals [1–3]. Since that time, and due to the large possible applications of this field, an extended community has grown up and considerable efforts have been devoted to photo-induce coherent acoustic phonons excitation in solids with a better and better efficiency and with a controlled acoustic frequency as well as phonon polarization [4]. Thermoelastic coupling driven by hot carriers has been observed in metals where strong (Ni, Cr), [5] as well as weak (Al [6], Au [7,8], Ag [8], Cu [8–10]) electron–phonon coupling metals have been investigated. Electron-acoustic phonon deformation potential as an efficient mechanism of coherent acoustic phonon generation has been studied in bare semiconductors [1,3,5,11–13] or in semiconductor superlattices where coherent acoustic phonon up to the THz frequency range have been generated [14–17]. Quantum wells, with efficient confinement of carriers, are also good candidates for generating CAP as recently reported [18–21]. Furthermore, materials with broken symmetry have permitted to control the emission of longitudinal as well as transverse coherent acoustic phonons [22–26]. Photoinduced inverse piezoelectric effect in semiconductors has received a great deal of attention too, since such investigations could pave the way for new optically-triggered piezoelectric transducers [22,25,27–29]. Finally the electrostriction has been shown to be an efficient mechanism in transparent solids [30,31] but only few demonstrations of this effect have been reported up to now [31,32]. We cannot briefly introduce the CAP generation process without mentioning the sound amplification effect found in quantum cascade lasers, named as "sasing effect" (phonon laser) [33] that will be specifically described in a review paper in this special issue of Ultrasonics Journal.

Beyond the development of new sources of coherent acoustic phonons, studying the photogeneration processes in solids, can also provide new physical insights on the electron–phonon coupling mechanisms in complex and correlated systems. The ultrafast acoustics is a time-domain technique and is complementary to the traditional methods of physical properties characterization such as

* Corresponding author.
E-mail address: pascal.ruello@univ-lemans.fr (P. Ruello).

http://dx.doi.org/10.1016/j.ultras.2014.06.004
0041-624X/

electronic transport (electrical conductivity, thermal conductivity) or optical elastic and inelastic spectroscopies (Brillouin and Raman light scattering, optical conductivity). For example, thanks to this time-domain spectroscopy, a special attention was paid the last decade to probe electron–phonon coupling in an important family of complex materials like oxides which are known to exhibit various phases transitions [34–41].

Beside the fundamental investigations on the generation processes and the physics of electron–phonon coupling, we cannot forget that a special care has continuously been taken for optimizing the detection processes which are crucial in this all-optical pump–probe spectroscopy [42–46]. Among recent achievements, it is now possible to probe lattice motion with time-resolved ultrafast X-ray diffraction experiments which offer complementary view on the ultrafast acoustic phonons dynamics [35,36,38–40,47].

In this review paper, we will focus on the ultrafast acoustics involving the use of femtosecond laser so that the frequency range of photogenerated coherent acoustic phonons will be GHz–THz. We invite the reader to refer to the review paper of A. Tam, for example, for lower frequency regime [48]. We describe separately each of the processes mentioned above, while, it is obvious, that in many circumstances several mechanisms contribute in the same time and with different amplitudes and phases. Even if some approaches are very similar concerning the description of the electron–phonon coupling mechanisms (deformation potential mechanism for example [49]), we will focus in this review only on coherent acoustic phonons and we will not discuss the photogeneration of optical phonons, even if this part remains an active domain of research and specially if we refer to the photoinduced coherent optical phonon involved in phase transitions [50]. We invite the reader interested by optical phonons photogeneration to read for example the review of Merlin [51].

This present review does not claim to be unique since some reviews have already been prepared in the past [4,52]. We have decided to focus on the physical origin while letting some mathematical descriptions to the more dedicated reference articles. We also have based our effort to present the more recent breakthrough in the field and to update as best as possible the references list of latest findings by the ultrafast acoustics community. This review is constructed as follows: the first part reminds the principle of a pump–probe experiment applied to the field of ultrafast acoustics. In the second part, we describe the microscopic mechanisms (thermoelasticity (TE), deformation potential (DP), inverse piezoelectricity (PE) and electrostriction (ES)) and in the last part we will discuss briefly some current orientations in the field of ultrafast acoustics regarding the photogeneration processes.

2. Principle of an ultrafast acoustics pump–probe experiment

The ultrafast optical experiment is historically based on the use of a femtosecond laser (100 fs) whose beam is split into two beams, namely the pump and probe beams. The first one is focused onto the sample to trigger a dynamics in a solid (liquid or gas are also studied with this technique). The second beam is also focused on the same region and its reflected light (or transmitted light) is collected by a photodiode. Because of the modification of the solid properties induced by the pump beam, the probe optical reflectivity changes. By adjusting the arrival time of the probe pulse (through a control of the optical path with moving mirror, see Fig. 1(a)), it is then possible to monitor in time the transient optical modifications of the solid with a very high temporal resolution. This technique works for studying different transient ultrafast phenomena, such as carriers relaxation, spin dynamics, thermal conduction, polaritons, coherent optical phonons and coherent acoustic phonons (CAP). The generation of coherent acoustic

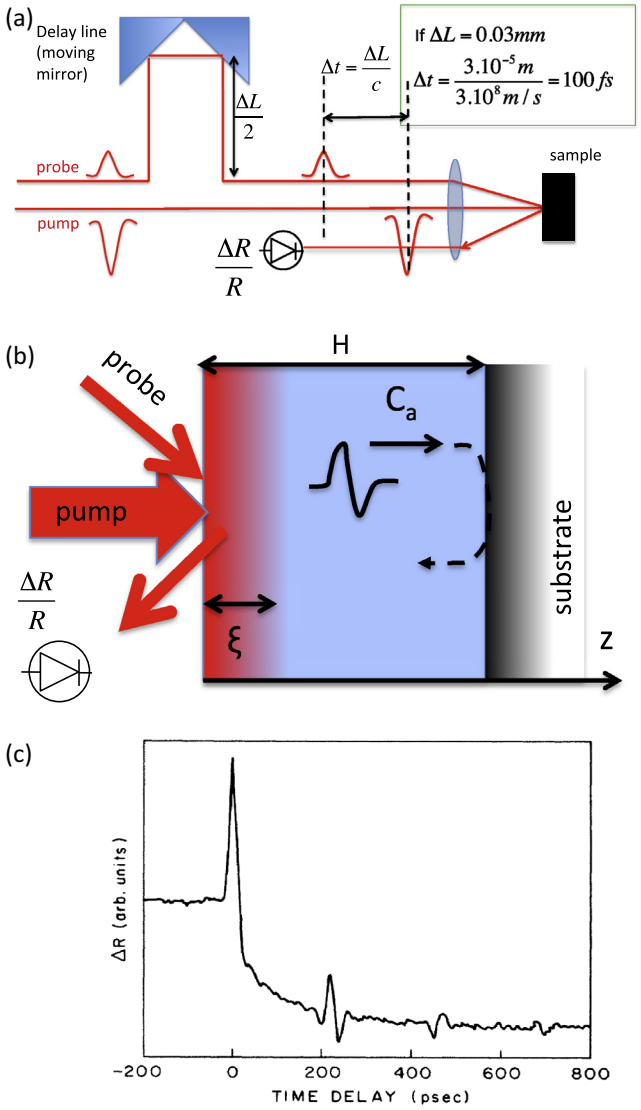

Fig. 1. (a) Schematic description of a pump–probe setup in the optical reflectivity geometry. The control of the optical delay path length ΔL of the probe beam allows to control the arrival time of the latter beam relative to the excitation beam (pump) and then to chose the temporal sampling of the transient optical reflectivity. (b) Sketch of the interaction of the pump beam with an opaque film giving rise to an acoustic pulse traveling forth and back at a sound velocity of C_a after mechanical reflections on mechanically free surface and film/substrate interface, respectively. ξ is the typical distance over which the absorbed pump energy is deposited. (c) Transient optical reflectivity obtained for a 220 nm thick As_2Te_3 film revealing three acoustic echoes whose spectral components provide informations on the early processes of opto-acoustic transformations in this semiconductor [3], Copyright (1986) by The American Physical Society.

phonons is based on the conversion of the optical energy of the pump beam into mechanical energy by the photoinduced stress denoted as $\sigma(z,t)$. This photo-induced stress that takes place over a characteristic depth ξ (Fig. 1(b)) depends on different parameters such as the material properties (optical, mechanical, thermal, ...) and the laser characteristics (wavelength, intensity, ...). Usually the pump and probe spot size is much larger than ξ so that the one dimension approximation is relevant at rather long propagation distance of CAP. In this description, the corresponding typical acoustic phonon pulse duration is given, as a first approximation, by the ratio of the depth ξ and the sound velocity C_a. It is worth to be mentioned that ξ may be different than the optical skin depth of pump radiation as we will discuss in part 3. To fix some orders, considering the deposited energy is confined only to a typical skin

depth of ~20 nm, this leads, with a sound velocity of 5000 m/s, to an acoustic pulse as short as a $\tau \sim 4$ ps, which corresponds to a characteristic frequency $f = \frac{1}{2\pi\tau}$. In some experiments, a film deposited onto a substrate is studied, so, in that particular case, the CAP, photogenerated on the free surface (Fig. 1(b)), travel forth and back within the film and several equidistant acoustic echoes can be detected in the transient optical reflectivity signal at arrival times $t = n \times 2H/C_a$, with $n = 1,2,\ldots$, C_a the sound velocity and H the film thickness, as shown in Fig. 1(c) [3]. The analysis of these echoes (temporal profile, arrival time, amplitude) provides direct information on the photoinduced strain mechanisms.

The equation of elastic motion that is usually employed in ultrafast acoustics is based on the classical approach of the wave physics, but the source term ($\sigma(z,t)$) has to be described following the quantum approach most of the time. So, this theory is a semi-classical theory. So, for an isotropic medium, the wave equation in one-dimensional (1D) geometry becomes:

$$\frac{\partial^2 u}{\partial t^2} - C_a^2 \frac{\partial^2 u}{\partial z^2} = \frac{1}{\rho} \frac{\partial \sigma(z,t)}{\partial z} \tag{1}$$

where u, ρ, σ are the material particle displacement, the mass density and the photoinduced stress that is composed of different contributions (DP, TE, PE, ES). The spectrum of the emitted acoustic phonon strain $\eta(z,t)$ can be theoretically found by applying integral transforms of this wave equation. It can be shown, for a semi-infinite system with a mechanical free surface ($\rho C_a^2 \eta(z=0,t) + \sigma(z=0,t) = 0$) that the acoustic strain spectrum is [4,52]:

$$\tilde{\eta}(\omega) = -\frac{i\omega}{2\rho C_a^3}\left(\hat{\tilde{\sigma}}\left(\omega, i\frac{\omega}{C_a}\right) - \hat{\tilde{\sigma}}\left(\omega, -i\frac{\omega}{C_a}\right)\right), \tag{2}$$

where $\hat{\tilde{\sigma}}(\omega, i\frac{\omega}{C_a})$ are the successive Fourier ($\tilde{\sigma}$) and Laplace ($\hat{\sigma}$) transforms of the photoinduced stress. The acoustic phonons spectrum is then completely governed by the dynamics of the source term. Depending on the mechanism, this dynamics (i.e. spectrum) is related to carriers transport, heat diffusion, electric field screening, for example. We will not derive the mathematical calculation of this spectrum in this review paper, since it has already been done [4,52] but we will mainly focus on the physical characteristic parameters and orders.

The detection of these CAP is then possible by analysing the variation of the reflected probe intensity, which is modified through the photoelastic effect (modification of the refractive index due to the presence of acoustic strain field, second term in Eq. 3) and through interferometric effect (CAP are able to displace surfaces and interfaces (first term of Eq. 3). For a semi-infinite medium ($z = [0, \infty[$), the transient complex optical reflectivity of the probe electric field component is then:

$$\Delta r/r = -2ik_0 u(0) + \frac{4ik_0 n}{1-n^2}\frac{\partial n}{\partial \eta}\int_0^\infty \eta(z,t) e^{2ink_0 z} dz \tag{3}$$

where $k_0, u(0), n$ and $\frac{\partial n}{\partial \eta}$ are the probe light wave vector in vacuum, the free surface displacement of the sample, the complex optical index and the photoelastic coefficient respectively. In a reflectometry geometry such as shown in Fig. 1(b), the magnitude of the transient intensity reflectivity is measured with $\frac{\Delta R}{2R} = Real(\frac{\Delta r}{r})$. We invite the reader to refer to more dedicated papers dealing with the detection processes [3,12,42–44,53]

3. Microscopic mechanisms involved in the ultrafast photogeneration processes in solids.

3.1. Deformation potential (DP)

3.1.1. Principle of DP

The deformation potential mechanism is the mechanism which relates the modification in energy of the electronic distribution to the strain in the solid. Generally speaking, as soon as the electronic distribution is changed (by the action of light or any external disturbance), and whatever the materials, there is at the microscopic level a modification of the interactions between cations and electrons, cations and cations and electrons and electrons. The interatomic forces are indeed completely dependent on the electronic distribution. If the interatomic forces are modified, this means that the equilibrium position in the lattice is also modified, so that, after some time, the crystal will be deformed, i.e. an acoustic phonon will be emitted. In the general books on solid state physics, this is often written as [49]:

$$\frac{\delta V}{V} = \frac{\delta U}{d_{eh}} \tag{4}$$

where d_{eh} (eV) is the deformation potential coefficient, U the electronic energy and $\delta V/V$ the strain caused by acoustic phonons (V is the volume). This equation underlines the direct link between the variation of the lattice strain and the electronic energy change. If one is modified, the second will be modified too, although with some time delay. Within the quantum point of view, we need to discuss the modification of the band structure. This deformation potential can be viewed like that: when atoms in a crystal exhibit relative displacements a strain ($\eta(z,t)$) appears (it can be longitudinal or shear strain). This strain modifies the orbitals overlapping since the atoms distance or bonds angle is varied and consequently this induces a shift of the electronic levels (δU). If the energy levels are shifted (up or down), electrons population adapt their energy following the quantum statistic law. As a consequence the electronic density at particular energy levels changes. On the other hand, when an electron travels in a crystal or electron–hole pairs are created, the local density of carriers at particular energy levels is thus modified (Fig. 2(a)). As a consequence, in this particular region, the strength of the atomic bonds changes, i.e. the atoms undergo a displacement: in other words, some phonons are then created or annihilated.

One can also adopt the molecular approach to understand the deformation potential mechanism. As depicted in Fig. 2(b), when carriers are excited by light, they are promoted towards empty electronic levels. Some new bonds are then created or destroyed but depending on the nature of the chemical bond (bonding, anti-bonding) this will either increase the equilibrium interatomic distance or diminish it. Some details concerning the mathematical formulation of the deformation potential are given in the following for the case of metals and semiconductors with experimental illustrations.

3.1.2. Experimental observations of photogeneration of CAP by DP

Metals: We can start by analysing the case of metals where some simplification of the electronic subsystem description can be done. In the Sommerfeld model, it is known that at thermodynamic equilibrium the electronic pressure is [55]:

$$P = \frac{2}{3}\frac{E}{V} \tag{5}$$

where E is the total kinetic energy of (nearly) free electrons and V the volume of the metal. A rapid calculation indicates that at thermodynamic equilibrium this electronic pressure is of the order few GPa. When these electrons are excited by the action of the laser, the

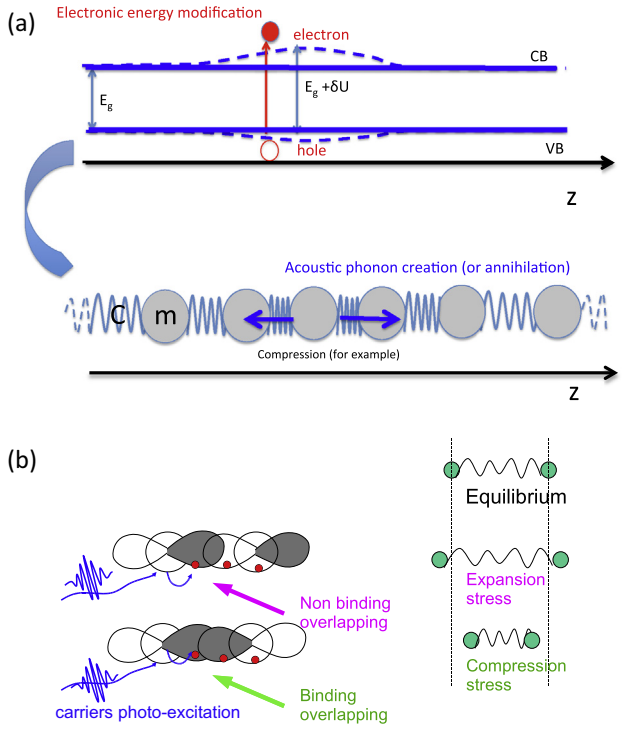

Fig. 2. (a) Deformation potential according to a band structure description: when the electronic distribution is disturbed (excitation of electron–hole pairs for example as shown), a modification of the interatomic interaction takes place which in turn forces the interatomic distances to change: this means that strain appears, i.e. phonons are created or annihilated. The example given here corresponds to a band structure of a semiconductor whose conduction (CB) and valence (VB) bands levels are shown by solid lines at thermodynamic equilibrium. Dashed line corresponds to the perturbed electronic levels after electron–hole pair formation. The symbol m is the atomic mass and C is the interatomic elastic stiffness for the 1D chain. (b) "Molecular view" of the deformation potential: the electrons are represented by red circles. The different colors of orbitals (white or grey) correspond to an opposite sign of the electronic wave functions. When orbitals are populated by light, bonding or antibonding interactions are switched on depending on the nature of these orbitals. This then forces cations to change their relative position after a given time leading either to a compression or an expansion of interatomic distances. (For interpretation of the references to colour in this figure legend, the reader is referred to the web version of this article.)

gain of energy becomes δE and the variation of pressure (photoinduced pressure) becomes then:

$$\delta P = \frac{2}{3}\frac{\delta E}{V} \tag{6}$$

We recognize $\delta E/V = C_e \delta T_e$ where C_e is the electronic heat capacity and T_e is the electronic temperature. This models considers that the electron–electron thermalization process is accomplished so that the electronic distribution is no more non-thermal and a Fermi distribution (i.e. a temperature T_e) can be defined to describe the hot electrons subsystem. Within this approximation [56], this leads to a new formulation of the photoinduced pressure as:

$$\delta P(z,t) = \gamma_e \frac{\delta E(z,t)}{V} = \gamma_e C_e \delta T_e(z,t) \tag{7}$$

In that case, the light-induced pressure is directly connected to change of electronic temperature and the electron Grüneisen coefficient γ_e, which is equal to 2/3 for the Sommerfeld model, but this is of course not the general case. The corresponding photoinduced stress becomes:

$$\sigma_{DP} = -\gamma_e \frac{\delta E(z,t)}{V} = -\gamma_e C_e \delta T_e(z,t) \tag{8}$$

One notices that the photoinduced stress σ_{DP} is negative when the quantum gas is heated, i.e. the metal will expand. If we take into account the existence of bands in the metal, the photoinduced stress has to take into account the light-induced modification of carriers population of different energy levels and that Grüneisen coefficient has to be associated to a given electronic k vector. The photoinduced stress becomes for an isotropic medium:

$$\sigma_{DP} = -\sum_k \delta n_e(k) E_k \gamma_k = \sum_k \delta n_e(k) \frac{\partial E_k}{\partial \eta} \tag{9}$$

where $\delta n_e(k)$ is the change of the electronic concentration at the level k. The Grüneisen coefficient is $\gamma_k = -\frac{1}{E_k}\frac{\partial E_k}{\partial \eta}$, with η the strain and $\frac{\partial E_k}{\partial \eta}$ the deformation potential parameter.

For metals, the spectrum of the deformation potential stress $\left(\widehat{\widehat{\sigma}}_{DP}\left(\omega, i\frac{\omega}{C_a}\right) = -\gamma_e C_e \widehat{\widehat{T_e}}\left(\omega, i\frac{\omega}{C_a}\right)\right)$ is related to the temporal evolution of the electronic temperature ($T_e(z,t)$). If we do not take into account the duration of electrons thermalization [56], one can then determine the transient electron temperature by solving, as a first approximation, the Two Temperature Model (TTM) equations which describe the transient change of the temperature (T_e) of the electron subsystem interacting with the lattice subsystem (i.e. phonons subsystem) temperature T_L [57], with:

$$\begin{aligned} C_e(T_e)\frac{\partial T_e}{\partial t} &= \kappa_e \frac{\partial^2 T_e}{\partial z^2} - g(T_e - T_L) + S(z,t) \\ C_L \frac{\partial T_L}{\partial t} &= g(T_e - T_L) \end{aligned} \tag{10}$$

where C_L, g, κ_e and S are the lattice heat capacity, the electron–phonon coupling constant ($g = 20$–60×10^{15} W m^{-3} K^{-1} for Cu [58] and $g = 200$–500×10^{15} W m^{-3} K^{-1} [59] for Ti for example), the heat conductivity (electronic) and the source term (spatial and temporal distribution of the laser light energy release). A typical time dependence of T_e and T_L is given in Fig. 3(a). However, the

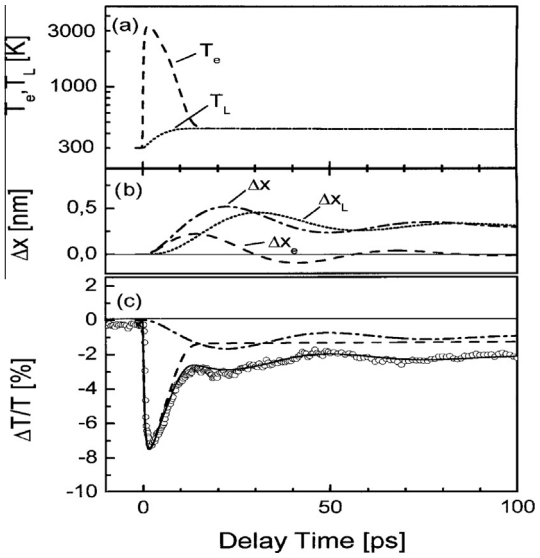

Fig. 3. (a) time dependence of the electron and phonon temperature predicted by the Two-Temperature Model (TTM) for metallic nanoparticles [54]. The excess of electronic pressure (i.e. deformation potential stress) exists in the metal as long as the electrons are not thermalized with the lattice (see the text). (b) Represents the calculated contributions of deformation potential and thermoelastic stress to the nanoparticles mechanical resonances (ΔX_e and ΔX_L refer to the DP and TE contributions to the NP vibration). Bottom figure shows the experimental transient optical transmission (the dotted-dashed curve is the acoustic contribution while the dashed curve is the electronic and thermal contributions to the transient optical transmission), Reproduced from Ref. [54], Copyright (2000) by The American Physical Society.

limitations of the TTM for the description of sound generation in metals with weak electron–phonon coupling were revealed in [6,60]. It was demonstrated that in such metals the thermalization time of the electrons, i.e., the time necessary for the establishing statistical Fermi–Dirac distribution of the electrons, which could be characterized by a parameter T_e, is comparable with the time of the energy release by overheated electrons to the lattice. It was demonstrated [60] that before electron thermalization the energy release by the electrons is controlled by specific characteristic time, which depends both on the electron–electron scattering time and electron–phonon scattering time. This characteristic time accounts for the multiplication of the energy-releasing electrons in the process of initially photoexcited electrons scattering by the Fermi sea of thermalized electrons. The multiplication process leads to the enhancement of energy release rate. Thus picosecond laser ultrasonics experiments were applied for the first time to estimate the duration of the femtosecond time scale process (characteristic time constant for the e–e scattering in gold was found to be 0.5 fs).

All these ultrafast thermalization processes rapidly diminish the hot electrons temperature, thus limiting the duration of the DP stress. Within the first ps, this DP mechanism is though more efficient [61] than thermoelastic process discussed later in Section 3.2 and very high frequency CAP can be emitted through DP. But these phonons are not so easily detected due probably to many reasons (acoustic attenuation, scattering by lattice imperfections). However, there are some situations where relevant observations of the existence of DP in photo-excited metals are reported. Most of these observations have been obtained in confined geometries where the hot electrons cannot diffuse rapidly out of the excitation region so that the electronic pressure remains quite important within a reduced volume of matter. These confined geometries are those obtained with nanoparticles or thin metallic films. One can cite the work of Perner et al. [54] (Fig. 3) where nanoparticles have been photoexcited and subsequent vibration eigenmodes have been observed. The understanding of the physical origin of the phase of the mechanical oscillation has been achieved only by taking into account the contribution of the electronic pressure additionally to the thermoelastic contribution. Other groups have also shown the importance of the electronic pressure in metal nanoparticles [62,63].

Semiconductors, oxide materials: In the case of solids with forbidden energy band separating occupied and non-occupied levels (semiconductors, oxides,), even if the physical origin of deformation potential is identical, the situation has to be described a bit differently. In solids with a forbidden band, the deformation potential mechanism will be usually important for roughly 1 GHz–1 THz CAP as soon as some electrons in the valence band are photoexcited towards the conduction band (holes are photogenerated in the valence band). The stress coming from the deformation potential mechanism given in Eq. (9) still holds as a general formulation. If we consider the limiting case where a solid with a band gap is photoexcited with a photon energy equal to the direct band gap (E_g), then the only relevant variation of electronic energy level will concern that of the band gap. As a consequence, Eq. (9) can be simplified as:

$$\sigma_{DP} = \sum_k \delta n_e(k) \frac{\partial E_k}{\partial \eta} = N \frac{\partial E_g}{\partial \eta} = -NB \frac{\partial E_g}{\partial P} = -d_{eh} N \tag{11}$$

where B and $N(z,t)$ are the bulk modulus and the photoexcited carriers concentration. This expression assumes an isotropic solid. In Eq. (11) the combination $B\frac{\partial E_g}{\partial P}$ provides the so-called electron–hole-phonon deformation potential parameter d_{eh}. It is also possible to distinguish the separate contributions to the deformation potential coupling of electrons (d_e) and holes (d_h) with:

$$\sigma_{DP} = -d_e n_e - d_h n_h = -d_{eh} N \tag{12}$$

where n_e and n_h are the carriers concentration at the bottom and top of the conduction and valence bands, respectively. For example for GaAs, $d_e + d_h$ = 9–10 eV [64] when electrons and hole are excited in the Brillouin zone center, i.e. with a photon energy close to the direct band gap (E_g = 1.43 eV). Depending on the nature of the electronic levels where the electrons (and holes) are photo-promoted, the lattice stress can be compressive or tensile. As an example of that non-trivial effect, when electrons are promoted in the Γ ($\partial E_g/\partial P$ = 10 eV Mbar^{-1}) and L valley ($\partial(E_L - E_\Gamma)/\partial P$ = 5.5 eV Mbar^{-1}) of GaAs, it contributes to an expansion of the crystal. On the opposite, it contributes to a contraction when electrons are promoted in the X valley ($\partial(E_X - E_\Gamma)/\partial P$ = −2.5 eV Mbar^{-1}). We remind that E_Γ is the highest energy in the valence band in the Brillouin zone center, E_L and E_X are the energy minima of the conduction bands situated respectively along the directions [1 1 1] and [1 0 0] in the Brillouin zone.

These electron–phonon coupling features are fully related to the nature of the orbitals overlapping in the crystals (bonding, non-bonding or anti-bonding). In the case of silicon, the deformation potential is negative with $\partial E_g/\partial P < 0$, so that a contraction of the lattice occurs under light illumination [65] (see Fig. 4(a)). On the opposite, a photoexcitation of electron–hole pair with a pump quanta having the same energy as the direct band gap in GaAs semiconductor leads to a deformation potential stress that is tensile (Fig. 4(b) [66]).

It is to be mentioned that if photon energy is larger than the band gap then we need to use the general expression Eq. (9). In

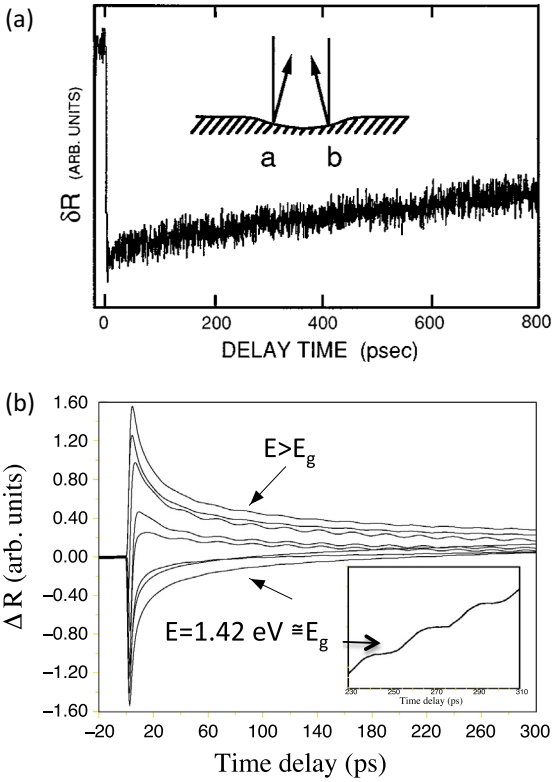

Fig. 4. (a) Ultrafast photoinduced contraction of silicon surface while it is illuminated by a femtosecond laser light with an energy of 2 eV. The detection of transient surface displacement is achieved thanks to a deflection method [65]. Reprinted with permission from [65], Copyright [1995], American Institute of Physics. (b) Generation of CAP in GaAs with variable pump energy. Even when the pump photon energy is equal to the band gap ($E = E_g$), some CAP are visible indicating that the driving mechanism of CAP emission is the deformation potential since the process depends only on the photoexcited electronic population in the bottom and top of the conduction and valence bands. It does not depend on the interaction of electrons with phonons (no intraband process for this particular optical excitation) [66].

that case, the deformation potential mechanism integrates different contributions related to different electronic levels that the excited electrons (holes) occupy before they totally relax towards the bottom of the conduction band (towards the top of the valence band). But because excited carriers usually relax very rapidly within intraband process (duration smaller than 1 ps typically [49]), Eq. (11) is often employed to account for the generation of CAP with frequency smaller than typically 1 THz. As it will be explained later, this intraband relaxation process will be responsible of incoherent phonons emission, which in turn will lead to the lattice heating (thermoelastic process presented in Section 3.2).

The analysis of carriers dynamics is essential to account for the spectrum of the deformation potential stress $\widehat{\widehat{\sigma}}_{DP}(\omega, i\frac{\omega}{C_a}) = -d_{e-h}\widehat{\widehat{N}}(\omega, i\frac{\omega}{C_a})$. This spectrum can be obtained by solving the space and time dependent equation of carriers dynamics which generally has the following form [4,52]:

$$\frac{\partial N}{\partial t} + \frac{N}{\tau_R} = D_{e-h}\frac{\partial^2 N}{\partial z^2} + \frac{\alpha(1-R_0)I}{h\nu}f(t)e^{-\alpha z}. \tag{13}$$

Here $N(z,t)$, corresponds to the concentration of photoexcited carriers which has already thermalized through intraband processes. The parameter τ_R is the recombination time and D_{e-h} is the carriers diffusion coefficient. The last term is the source term describing the initial process of increase in concentration of photoexcited carriers due to the absorption of optical quanta $h\nu$ (α is the pump light absorption coefficient and R_0 the optical reflectivity of the sample at the wavelength of the pump photon and $If(t)$ ($W.m^{-2}$) is the pump light intensity temporal variation). The boundary conditions are determined by the carriers dynamics at the surface, like surface recombination, with $D_{e-h}\frac{\partial N}{\partial z}|_{z=0} = S_r \times N$, where S_r is the surface recombination (radiative or non-radiative) velocity [65].

Several detailed experiments have been performed in which the deformation potential has been shown to be the driving mechanism in bare semiconductors and the effect of carriers dynamics (τ_R, D_{eh}) on the emitted CAP spectrum has been discussed and modeled [3,11–13,67]. In case of strong near-surface absorption of pump laser radiation in semiconductors, the diffusion of plasma across the light penetration depth could take less time than for the sound propagation across it. In other words, plasma diffusion can be supersonic at the time scale of interest and can importantly broaden spatial distribution of the photo-induced DP stress from the sound generation point of view. In this case, an additional characteristic time, which is equal to the time D_{e-h}/C_a^2 of plasma deceleration down to sound velocity, could clearly manifest itself in the profiles of the photo-generated acoustic pulses [53,68]. The broadening of the leading front of the photo-generated acoustic pulse, caused by the supersonic diffusion of the e–h plasma, was first observed in Ge [67,69]. Later the manifestations of the supersonic diffusion of e-h plasma were documented in the experiments with GaAs [11–13].

Furthermore, because of the difference in the magnitude of deformation potentials of the electrons and holes, the DP mechanism of sound generation is sensitive to their possible separation in space. In the recent picosecond ultrasonics experiments in p-doped GaAs [27] important suppression of the sound generation by DP mechanism was caused by suppression of the diffusion of the photo-excited electrons by the built-in electric field directed from the surface and pushing the electrons towards the surface. The sound generation by DP which is much more efficient for electrons, is then confined to the near surface. But this process efficiency is strongly reduced because of interferometric cancellation of the anti-phase acoustic waves propagating in the bulk of GaAs after reflection and without reflection from the surface [27]. This important suppression of the DP mechanism in p-doped GaAs is in contrast to the case of n-doped GaAs [28], where the direction of the built-in field is opposite and localization of the photo-excited holes near the surface has weak influence on the total efficiency of DP mechanism. The competition between deformation potential mechanism and inverse piezoelectric one will be discussed in Section 3.3.

The carrier lifetime (τ_R) has an important role too. Recombination of the e–h pairs suppresses DP mechanism of sound photogeneration at cyclic frequencies which are lower ($\omega < 1/\tau_R$) than the inverse recombination time [4,52,68]. In the case of nonlinear non-radiative e–h recombination, for example Auger recombination, the increase of the e–h plasma concentration with increasing pump laser fluence diminishes the recombination time (Fig. 5(a)). This causes the suppression of the DP mechanism which is accompanied by accelerated heating of the lattice and, thus, by the increased generation of sound by TE mechanism. Transition with increasing pump laser fluence from the sound generation by the DP mechanism to its thermoelastic generation was first reported in the experiments with nanosecond laser in Si a long time ago [70]. The manifestations of this transition in picosecond laser ultrasonic experiments in GaAs has been reported for the first time quite recently [13] (Fig. 5(a)).

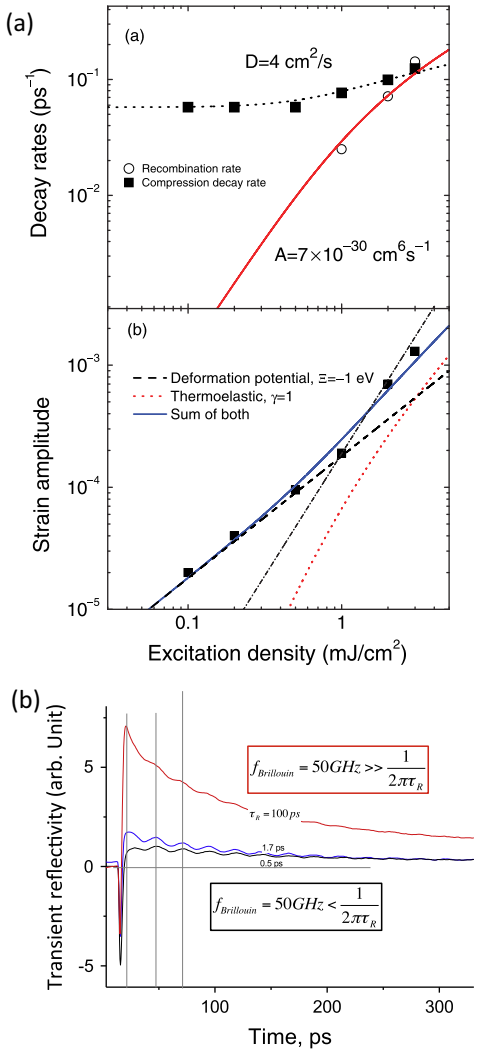

Fig. 5. (a) Pump fluence dependence of the Auger recombination rate and of the deformation potential strain amplitude in GaAs semiconductor [13]. Copyright (2013) by The American Physical Society. (b) Transient reflectivity signal obtained in LT-GaAs (pump 400 nm, probe 800 nm) with variable carrier non-radiative recombination time τ_R [72]. Generation of 50 GHz CAP is governed by the deformation potential process only for sample having long lifetime carrier (100 ps), while thermoelastic process becomes dominant for short carrier lifetime samples.

Additional illustration of this phenomenon is obtained with LT-GaAs (low Temperature grown GaAs). Because of defects in the band gap, the recombination time can be as fast as few ps as shown in Fig. 5(b) [71]. In that case, for sample having a recombination time of τ_R = 100 ps, the CAP at 50 GHz is mainly driven by the deformation potential [72]. On the opposite, for short recombination time (τ_R = 1.7 ps and 0.5 ps), the CAP at 50 GHz is mainly driven by thermoelastic (TE) mechanism.

Much higher CAP frequencies than those discussed previously can be also obtained by deformation potential process. One of the most popular approaches is to use the superlattice for phonon dispersion folding [14,15,17]. Several experiments have been conducted in the last 15 years and only one example is shown in Fig. 6(a and b) [14]. In these situations the deformation potential stress follows the periodicity of the superlattice permitting advanced control of the emitted as well as detected acoustic phonons modes. Broadband acoustic pulse of ~ 5 ps in duration has also been observed in bulk semiconductor [12] (Fig. 6(c)) even with deeply penetrating pump beam photon (~1000 nm) leading to a Heaviside-like photogenerated acoustic front. In this particular situation, high frequency components of CAP actually exist because of the sharpness of this leading acoustic front and are efficiently detected thanks to a probe beam strongly absorbed near the surface (~16 nm) allowing a broadband detection. Finally, recent observations of the photogeneration of CAP by the deformation potential mechanism have been reported in quantum wells and quantum dots [19–21] Fig. 6(d). Since the carriers are intrinsically localized and with a well defined electronic energy, the objective is to get selective optical excitation of electronic level to control the spectrum of the CAP emission, i.e. to imprint the electronic wave function form onto the emitted CAP strain.

3.2. Thermoelasticity (TE)

3.2.1. Principle

As the title indicates, thermoelasticity is a phenomenon involving the temperature and the elasticity of a solid. Since it is commonly understood that laser can heat samples, and it is even easy to check it experimentally (at least in static regime), this mechanism is well known in the community of laser ultrasonics and has been already fully described elsewhere in previous review (kHz, MHz regimes are discussed in Ref. [48]).

To induce a volume change under temperature increase, i.e. thermal expansion, lattice anharmonicity is necessary [55]. The reciprocal effect is also possible with a lattice temperature increase in the matter induced by the presence of an acoustic field. As sketched in Fig. 7(a), the mean lattice parameter $r(T)$ increases when vibrational energy is elevating (i.e. increase of phonon population) only if the interatomic potential is anharmonic (r_0 is the lattice parameter at T = 0 K). This consideration is general and independent on the process of lattice heating (electronic energy release by intraband electron–phonon coupling, by non-radiative interband recombination). The thermoelastic strain caused by thermal expansion is $\eta = \delta V/V = 3\beta B\delta T_L$, where β is the linear thermal expansion coefficient and δT_L is the lattice temperature increase. The associated increase of internal pressure, called thermoelastic pressure, becomes:

$$dP_{TE} = 3B\beta\delta T_L \tag{14}$$

The integration of this equation provides the variation of the thermoelastic (TE) stress according to:

$$\sigma_{TE} = -3B\beta\Delta T_L \tag{15}$$

From the microscopic point of view, the lattice heating comes from the energy transfer from the initially excited electrons towards the phonons sublattice (see Fig. 3(b) for the TTM model applied to a metallic system). The hot carriers interact indeed with phonon to relax towards lower energy levels. When the relaxation processes take place acoustic phonons are emitted (depending on the solid, either optical or/and acoustic phonon are emitted and optical phonons can also decay into acoustic phonons). These emitted phonons have no phase relation between each other, so that they contribute to the increase of the population of thermal phonons. The calculation of the pressure induced by a modification of the phonon

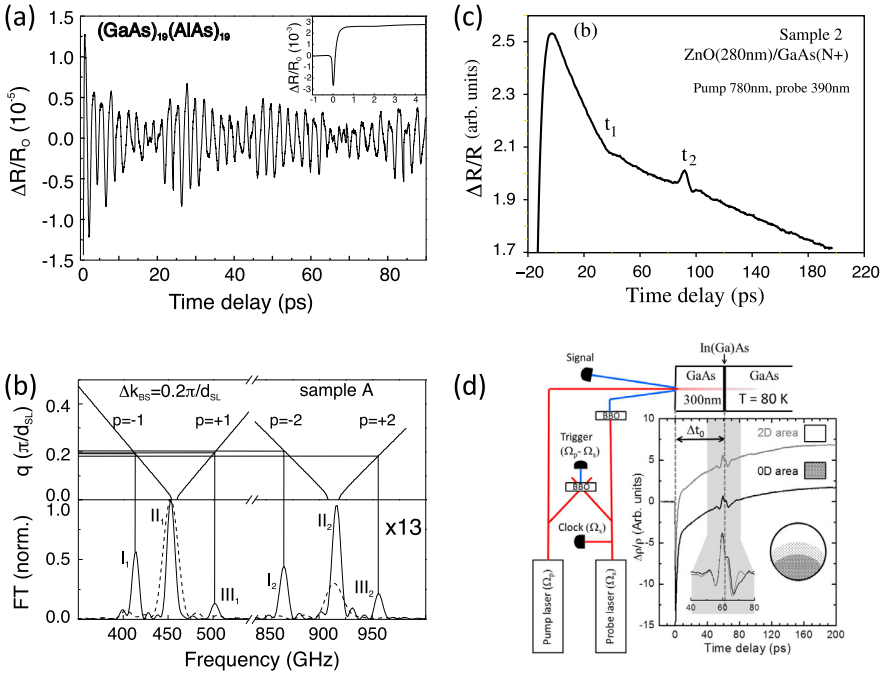

Fig. 6. (a) CAP in a semiconductor superlattice [14], Copyright (1999) by The American Physical Society. (b) Detection of CAP up to the THz range in mode folded semiconductor superlattice, Copyright (1999) by The American Physical Society. (c) Short acoustic pulse photogeneration in GaAs semiconductor covered by ZnO film [12], Copyright (2010) by The American Physical Society. The ZnO layer acting as an acoustic-delay line permits to distinguish in the time domain the detection of the short acoustic pulse at a delay t_2. (d) Photogeneration of CAP in quantum dots [21]. Reprinted with permission from [21], Copyright (2013), American Institute of Physics.

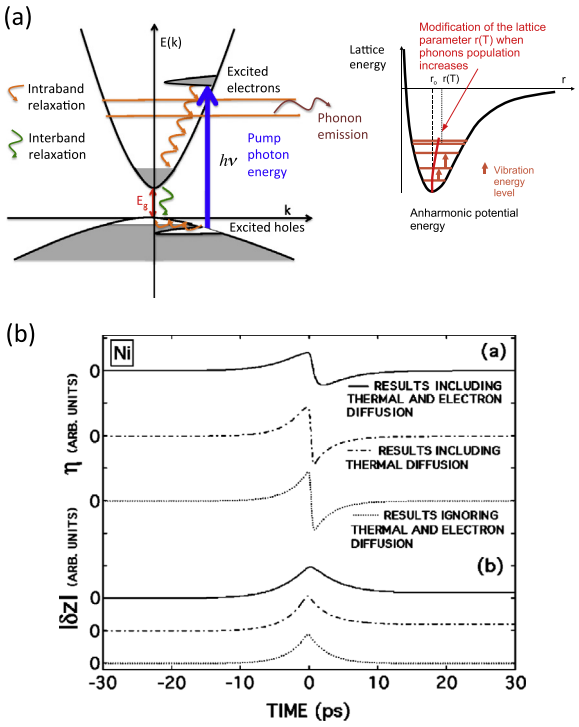

Fig. 7. (a) Left part: schematic view of the intraband relaxation process (red arrows) which leads to incoherent phonon emission which contributes to the local increase of the phonon pressure. The interband process is sketched by the green arrow. Right part: modification of the mean interatomic distance $r(T)$ when the vibrational energy increases in an lattice anharmonic potential. (b) CAP emitted by thermoelastic process in strong electron–phonon coupling metal Ni [5]. The lattice and electron heat diffusion have a weak influence. Copyright (2003) by The American Physical Society. (For interpretation of the references to colour in this figure legend, the reader is referred to the web version of this article.)

population ($n_p(\vec{k})$) has been derived in classical books of solid state physics [55] or physical acoustics [73] and we have a general expression:

$$\sigma_{TE} = -\sum_k \delta n_p(k)\hbar\omega_k\gamma_k^p = -\gamma_L C_L \delta T_L(z,t) \tag{16}$$

where γ_L is an averaged Grüneisen coefficient among all k-dependent Grüneisen factors $\gamma_k^p = -(V/\omega_k^p)(\delta\omega_k^p/\delta V) = -(1/\omega_k^p)(\delta\omega_k^p/\delta\eta)$. $C_L\delta T_L$ corresponds to the change of lattice vibrational energy $\sum \delta n_p(k)\hbar\omega_k$. In metals, once the electrons and phonons have thermalized (see in Fig. 3(a) the dynamics of thermalization in the frame of the TT model), the lattice temperature can be estimated roughly by assuming a complete transfer of energy from the electron to the phonon subsystem with $\delta T_L = Nh\nu/C_L$, where N is the photoexcited carriers concentration, C_L the lattice heat capacity and hν the pump quanta energy. In the case of semiconductors, as depicted in left part of Fig. 7(a), ultrafast lattice heating is connected to the intraband relaxation process of electrons (holes) in the conduction (valence) band and is: $\delta T_L = N(h\nu - E_g)/C_L$, where E_g is the band gap. This calculation does not account for possible interband relaxation processes, so that only a part of the absorbed energy is converted into heating. The photoexcited carriers accumulated at the bottom and top of the conduction and valence band contribute to the deformation potential stress as discussed in previous Part 3.1 (see Eq. (11)). If the carriers undergo non-radiative interband relaxation process (non-radiative recombination), then we have to take into account an additional source of lattice heating which is $\delta T_L = NE_g/C_L$, where E_g is the band gap.

3.2.2. Experimental observations of photogeneration of CAP by TE process

Metals: While deformation potential is usually more easy to evidence in semiconductors, thermoelastic process has been the most widely involved mechanism in photoexcitation of metals. For photogenerated sound with frequency up to hundreds of GHz (period much longer than the electron–phonon coupling time), it is indeed the dominating mechanism [61]. We have mentioned previously how rough estimate of the lattice heating can be achieved. It is worth to mention that the heating of the lattice by hot carriers can occur at different spatial scale according to the distance over which the electrons can deposit their energy, and this will control the acoustic spectrum $\left(\widetilde{\widehat{\sigma}}(\omega, i\frac{\omega}{C_a}) = -3B\beta\delta\widetilde{\widetilde{T_L}}(\omega, i\frac{\omega}{C_a})\right)$. We then have two important cases. In the case of strong electron–phonon coupling metals, where the lattice is immediately heated indeed (within less than 1 ps [74]), we can consider with a good approximation that hot electrons remain nearly in the region of the pump light absorption (the characteristic distance over which the electrons deposit their energy into the lattice $L = \sqrt{(\kappa_e/g)}$, where κ_e is the electronic heat conductivity and g the electron–phonon coupling [9], is of the same order as the optical skin depth of pump light). This has been demonstrated in the case of Ni for example [5] (See Fig. 8(a)) but also observed in Co [75]. To account for quantitative description, the space and time dependence of T_L (Eq. (17)), controlled by the lattice heat diffusion (D_L is in general a combination of electrons and phonons contributions) has to be found to get the spectrum of the thermoelastic stress.

$$\frac{\partial T_L}{\partial t} = D_L\frac{\partial^2 T_L}{\partial z^2} + \frac{\alpha(1-R_0)I}{C_L}f(t)e^{-\alpha z}. \tag{17}$$

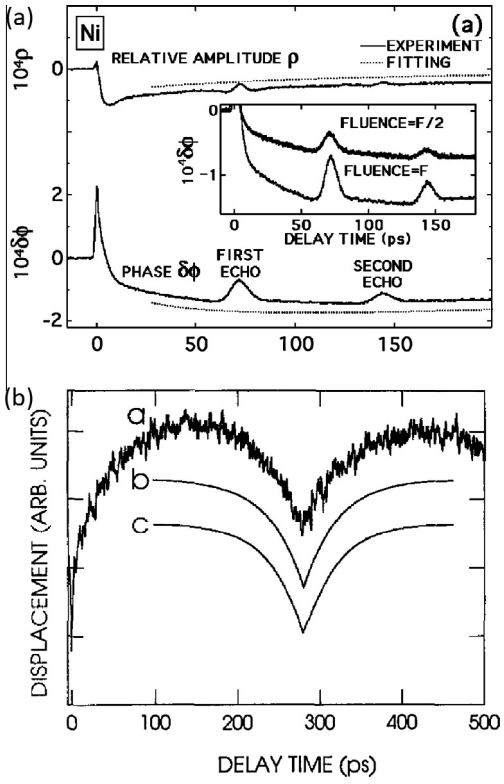

Fig. 8. (a) photogeneration of CAP by thermoelastic process in strong electron–phonon coupling metals [5], Copyright (2003) by The American Physical Society. (b) Very large broadening of the emitted acoustic pulse (i.e. spatial broadening of the lattice heating) in weak electron–phonon coupling metal (gold) due to rapid diffusion of hot carriers [7]. Copyright (1996) by Elsevier.

This complete calculation has been done for the nickel for example (Fig. 8(a)) where pretty high frequency CAP are observed. The situation is different for weak electron–phonon coupling metals. In that case the role the hot carriers diffusion is important. For these weak electron–phonon coupling metals (noble metals where the electron–phonon coupling time is roughly one order larger than that in strong electron–phonon coupling metals), diffusive transport of hot carriers occurs within hundreds of femtoseconds over distance much larger than the skin depth of pump light. The typical distance over which electrons transfer their energy to the lattice $L = \sqrt{(\kappa_e/g)}$, can be as large as 100 nm in gold and copper [7,9,10]. In that case the spatial profile of the emitted acoustic pulse is mainly governed by the profile of hot electrons energy release and neither by the pump light absorption coefficient α, nor by the lattice heat diffusion. In this particular situation, the profile of the strain pulse generated near mechanically free surface is very close to $\eta(z,t) \sim -sign(z-Vt)exp(-\sqrt{g/\kappa_e}|z-Vt|)$. This has been demonstrated experimentally in gold [7] and copper [9,10].

Even if the generation of acoustic pulse is well understood in bare metals, there is however some not completely understood ultrafast heating processes in metals involving the interaction of fast hot carriers with buried metallic interfaces. Some experimental observations have reported the emission of CAP at aluminum/photoresist substrate [6] and at copper/titanium interface [10] but opened questions remain about the real opto-acoustic conversion mode. The current problem maybe related on necessity of a precise description of the electronic and lattice temperature profile at a bi-metallic interface where probable electronic and thermal phonons interface resistance effects exist.

Furthermore, because large size metal single crystals can be obtained and cut according to different orientations, thermoelastic generation in metals with broken symmetry has been proved to be efficient to generate shear acoustic phonon as reported in disoriented Zn single crystal (Fig. 9). Since the employed metals had quite large electron–phonon coupling constant, no significant broadening of the emitted acoustic pulse was observed which ensured to achieve quite high frequency shear phonon emission up typically to 50 GHz [22–24]. Some special growing process control of canted metal films has also permitted to disorient the eigen axis of iron crystal relative to the normal of the irradiated surface so that it was possible to generate shear phonons [76]. Moreover, shear coherent acoustic modes can also be obtained by mode conversion of LA phonons at surface or interface as shown by different research groups [77–79].

Semiconductors: We have mainly discussed the case of metals and only a little that of semiconductors. One reason is the dominating contribution in many semiconductors, at the GHz–THz frequencies under consideration here, of the deformation potential. As stated in Section (3.1), that deformation potential is efficient as soon as the lifetime of the photoexcited carriers is longer than the inverse of CAP cyclic frequency. As shown in Fig. 5(a), the thermoelastic process can prevail as soon as the deformation potential is suppressed by fast carriers recombination that can be enhanced either by increasing pump fluence [13] or by the presence of high concentration of intra-gap defects [72] (Fig. 5(b)).

3.3. Inverse piezoelectric process (PE)

3.3.1. Principle

In non-centro symmetric materials [80], there is a coupling between the strain (η) and the macroscopic electric field (E) that can exist inside a material. This coupling comes from the possible separation of the barycenter of positive and negative charges when a lattice is submitted to a strain. This means that a strain induces a macroscopic polarization P. Different thermodynamic relations exist to account for these phenomena [80]. The direct piezoelectric

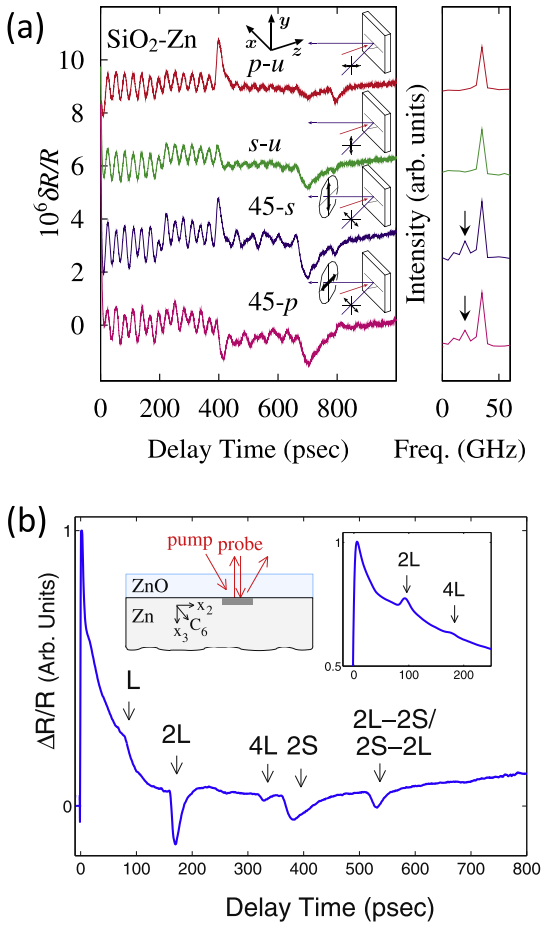

Fig. 9. (a) Transient optical reflectivity obtained in disoriented Zn single crystal covered by SiO_2. The FFT of the Brillouin oscillations reveals the presence of LA but, although weaker in amplitude, TA modes [22], Copyright (2004) by The American Physical Society. (b) Broadband LA and TA acoustic pulses observed after optical excitation of disoriented Zn single crystal covered by ZnO. Mode-converted acoustic pulses are also visible (2L–2S and 2S–2L) [23]. Copyright (2007) by The American Physical Society.

effect (characterized by the tensor d_{ij}) corresponds to the appearance of a polarization while the material is submitted to an external stress and is written in contracted tensorial form as:

$$P_i = d_{ij}\sigma_j, \tag{18}$$

where $i = 1, 2, 3$ and $j = 1,2,\ldots,6$. The inverse piezoelectric effect (characterized by the tensor p_{ij}) corresponds to the appearance of an internal strain when the material is submitted to an electric field and is written as:

$$\eta_j = p_{ij}E_i \tag{19}$$

There also exists a relation between the electric field and the induced stress such as:

$$\sigma_j = e_{ij}E_i, \tag{20}$$

where piezoelectric moduli e_{ij} is around 0.1–0.2 C m^{-2} in GaAs [64] while it is up to two orders of magnitude larger in ferroelectrics [81]. These piezoelectric properties are widely used in research and a lot in industry through the use of piezoelectric transducers for non destructive testing. Perovskite family, such as PZT, PMN materials are among the most employed materials [81]. These materials are sources of acoustic waves when they are submitted to an external bias. The current limitation of the frequency range of these electrically-driven piezo-transducer is around GHz. As we

will see below, by employing light one can overcome this limitation and optically-driven piezo-transducer open new possibilities for the high frequency regime (GHz–THz). As we will see, the light-controlled piezoelectric (PE) mechanism has peculiar properties compared to two other processes described before, i.e. DP and TE mechanisms. If the electric field changes its direction ($E > 0$ or <0) then the photoinduced stress also changes its sign. If an electric field is applied for two opposite crystallographic orientations of the sample the stress will change its sign as well. The latter property deeply contrasts with the thermoelastic or deformation potential processes where a 180° change of a crystallographic orientation does not change the associated stress. This property is related to the fact that piezoelectric tensor is 3rd rank tensor while $(d_{eh})_{ij}$ (deformation potential tensor) and β_{ij} (linear thermal expansion coefficient involved in the thermoelastic process) are 2nd rank tensors.

There are different situations where a macroscopic electric field can exist in a material: external application of a bias, pre-existing built-in field in the vicinity of semiconductor surface or in a hetero-junction, generation of an electric field by dynamic separation of electrons and holes (Dember electric field). There is also the internal polarization existing within the ferroelectric domains [81]. For semiconductors such as GaAs or GaN the buit-in filed (BIF) is often rather high with typical value of 100–500 kV cm^{-1} [64]. In Fig. 10 is shown a sketch of the electronic band structure close to a surface of a semiconductor where surface defects can trap the majority carriers and hence induce the appearance of a surface charge. A macroscopic electric field exists then close to the surface. The extension of this electric field is given by $L_{BIF} = \sqrt{\frac{2\epsilon\epsilon_0 V_{BIF}}{n|e|}}$, where V_{BIF} is the built-in potential (typically 0.5–1 eV in GaAs depending on the defects [64]), e is the elementary charge, ϵ is the relative the dielectric constant of the solid and n the majority doping carriers concentration). The built in field is $E_{BIF} \sim V_{BI}/L_{BIF}$. We invite the reader to refer to a general book on semiconductors to have details about this built-in electric field physics [82].

In ultrafast acoustics experiments, the pump laser beams photoexcite charge carriers in the region of pre-existing field. As a consequence, these carriers can screen the macroscopic electric field. According to Eq. (20), the changes in electric field induce stress through the inverse piezoelectric effect. This forces the atoms to move, which means that acoustic phonons are emitted. The source of acoustic phonons is directly connected to the transient electric field that has time and space dependence $E(z,t)$. This time and space dependence are connected to the dynamics of carriers that can be found according to the classical electrodynamic equations (motion of carriers and Poisson equation) [52].

$$\frac{\partial n_{e,h}}{\partial t} \mp \mu_{e,h}\frac{\partial (n_{e,h}E)}{\partial z} - D_{e,h}\frac{\partial^2 n_{e,h}}{\partial z^2} + \frac{n_{e,h}}{\tau_{e,h}} = \alpha N_L f(t) e^{-\alpha z}$$

$$\frac{\partial E}{\partial z} = -|e|\frac{(n_e - n_h)}{\epsilon\epsilon_0}$$

where $n_{e,h}, \mu_{e,h}, D_{e,h}$ and N_L are the concentration, mobility, diffusion coefficient of electrons (e) or holes (h) and the photoexcited carriers sheet density.

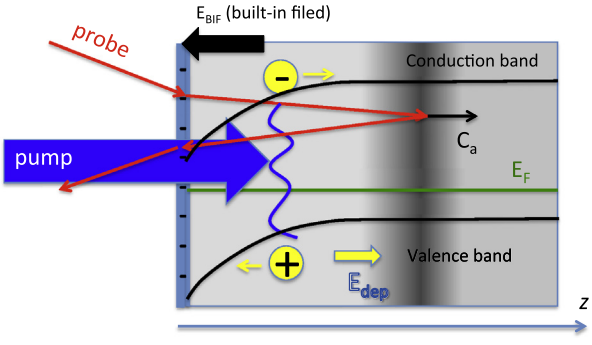

Fig. 10. When majority carriers are trapped at the surface of a semiconductor (surface states), surface charges appear (negative charge in the case of the example of a n-doped semiconductor) which in turn leads to the formation of a depletion layer with an associated electric built-in field E_{BIF} [82]. When electron–hole pairs are photogenerated (yellow disks), they are separated in E_{BIF} and form a depolarizing field $E_{dep.}$ which then reduces the total electric field. This gives rise to an inverse-piezoelectric stress which then is a source of emission of acoustic phonons (sound velocity C_a). (For interpretation of the references to color in this figure legend, the reader is referred to the web version of this article.)

3.3.2. Experimental observations of photogeneration of CAP by PE process

Several observations of the GHz coherent acoustic phonon (CAP) generation by the inverse piezoelectric field have been reported during the last 15 years. Among them one can cite the generation of CAP by injecting carriers within the built-in field of a p–n junction [83]. In Fig. 11(a), the transient reflectivity signal is shown for a p–n junction irradiated with a near UV pump beam

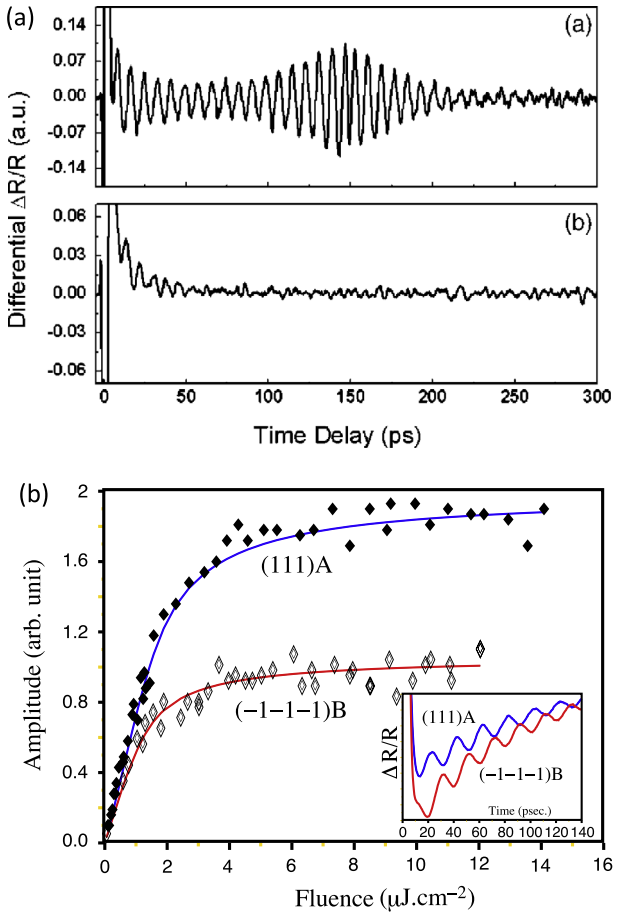

Fig. 11. Photogeneration of CAP by the inverse piezoelectric effect (a) in a GaN p–n junction. The acoustic pulse observed (top figure) at a time delay of 150 ps comes from the emission of CAP from the buried p–n junction. If the pump photon energy is too high (bottom), the light is mainly absorbed in the near surface and does not photoexcite charge carriers within the p–n junction and no CAP are emitted [83]. Reprinted with permission from [83]. Copyright (2012), American Institute of Physics. (b) Photoexcitation of CAP by inverse piezoelectric effect in piezoactive [111] GaAs wafer. The sign of the emitted acoustic strain changes when the crystallographic direction is reversed from A to B [27]. Reprinted with permission from [27]. Copyright (2010), American Institute of Physics.

very close to the GaN band gap (3.4 eV) permitting injection of carriers into the buried p–n depletion layer (the junction is situated around 1 μm beneath the free surface and the pump beam penetration depth $1/\alpha$ is around 700 nm). In that case, an acoustic pulse is observed at $t \sim 150$ ps, which is equal to the propagation time of acoustic phonons from the p–n junction to the free surface where they are detected (mainly the Brillouin component at 110 GHz was detected). On the other hand, if the pump beam energy is too high (bottom inset of Fig. 11(a)) the pump light does not penetrate up to the p–n junction and acoustic pulse is generated on the free surface only. It is crucial to note that the magnitude of the acoustic pulse detected at $t = 150$ ps is comparable to the amplitude of acoustic pulse generated at the free surface. Because, of a decaying carriers concentration in depth due to the exponential profile of the pump energy absorption, this pulse cannot originate then from the deformation potential or thermoelastic mechanisms contributions which both are proportional to the absorbed energy. Only PE mechanism due to the electric field pre-existing mostly near the p–n junction and not on the surface of the sample, can account for the observations. These results clearly show that the photoexcited carriers screen the junction field and, through inverse piezoelectric field, lead to the generation of CAP. Another illustration of the clear origin of the piezoelectric effect comes from the analysis of time-resolved Brillouin signal in a highly p-doped GaAs [1 1 1] crystal (Fig. 11(b)). In this case, due to the p-doping, the preexisting built-in field is orientated from the surface towards the inner of the sample whatever the face we consider (face A (1 1 1) or B $(-1-1-1)$). As a consequence, when photoexcited carriers are injected near the surface (pump wavelength at 400 nm penetrates around 15 nm beneath the surface), there is a rapid screening of the built-in field but since the piezoelectric constant is of opposite sign for the face A and B, the emitted Brillouin signal exhibits a π phase shift. Additional experimental evidences of the inverse piezoelectric effect have also been reported in n-doped GaAs [28] and in InGaN/GaN superlattice [16].

Furthermore, it had been expected [52,53] that in piezoelectric semiconductors with a built-in electric field spatial scale of the photo-induced PE stresses could be controlled by the width of charge depletion region rather than by the length of pump laser light penetration. These theoretical predictions has been confirmed by the recent experiments in doped GaAs [27,28], where in case of the blue pump radiation the light penetration depth is shorter than the depletion zone [27], while in the case of red pump radiation the light penetration depth is larger than the depletion zone [28], but in both cases the width of the depletion zone has manifested itself in the sound generation process. In particular, in case of the PE generation of sound, the maximum efficiency of the opto-acoustic conversion and the maximum acoustic amplitude achievable at Brillouin frequency, both are controlled by the non-dimensional parameter equal to the product the depletion width and the acoustic wave number at Brillouin frequency [27]. As an important result for future applications, it is worth to mention that CAP generation by the inverse piezoelectric effect can be tuned with an external bias [84,85]. In Fig. 12(a), one can see that variable bias permits to clearly enhance the magnitude of the longitudinal acoustic (LA) mode (109.5 GHz) in InGaN/GaN multiple quantum wells. The origin of the lower frequency mode (67.7 GHz) whose amplitude is much smaller that of the LA mode was not established and is still being under investigation. Finally, even in the absence of pre-existing electric field (surface built-in electric field, junction electric field or external bias), it is possible to generate CAP by the inverse piezoelectric effect. The required sample must be non-doped with a very low level of doping (impurity) concentration to prevent any formation of large surface built-in field. In that case, PE mechanism can be achieved with Dember electric field that arises from the separation in space of positive and negative

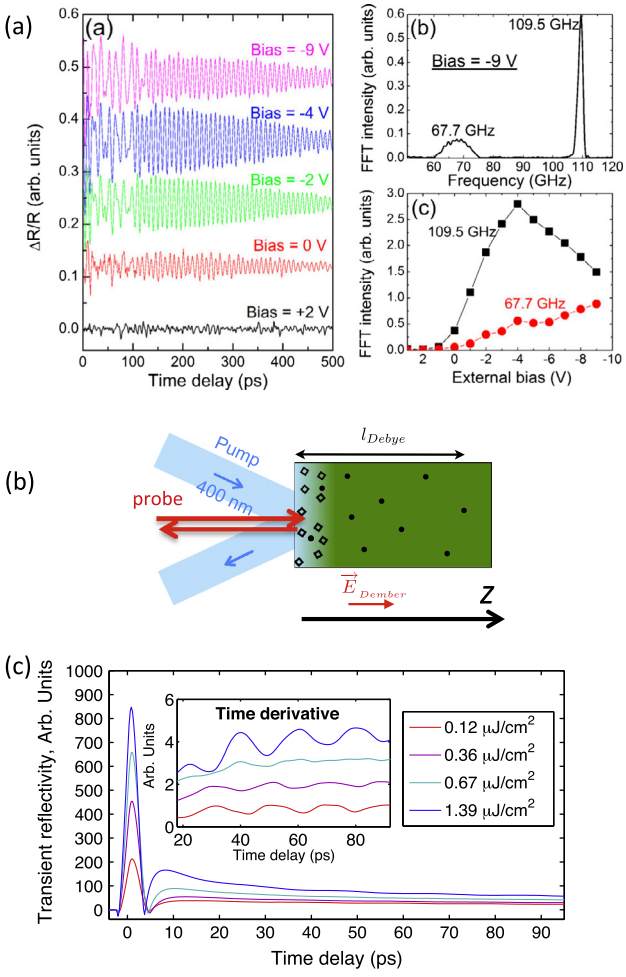

Fig. 12. (a) Longitudinal acoustic mode (109.5 GHz) photogeneration by piezoelectric coupling in multiple quantum-well InGaN/GaN as a function of external bias [85]. Reprinted with permission from [85]. Copyright (2012), American Institute of Physics. (b) Schematic representation of the appearance of the Dember electric field at low pump fluence (non-ambipolar regime) due to a higher mobility of electrons (black dots) that of holes (white cubes). Adapted from Ref. [87]. (c) Pump power dependence of the Brillouin signal in non-doped GaAs. At low fluence the CAP photogeneration is governed by the inverse piezoelectric effect driven by Dember electric field while at high pump fluence, the deformation potential prevails [87].

photo-excited charges due to difference between electron and hole diffusivities (Fig. 12)) and is related to the photoexcited carriers sheet density N_L at low fluence (Fig. 12(b)):

$$E_{Dember}(z,t) = \frac{\frac{|e|N_L}{\epsilon\epsilon_0}}{1 + z/L_{Debye}}, \tag{21}$$

with $L_{Debye} = \frac{2kT\epsilon\epsilon_0}{|e|^2 N_L}$ the Debye screening length. At high pump fluence, in the ambipolar diffusion regime [86,87], the Dember electric field becomes:

$$E_{Dember}(z,t) = -\frac{(D_e - D_h)}{\mu_e - \mu_h}\frac{1}{n}\frac{\partial n}{\partial z} = \alpha\frac{kT}{|e|} \tag{22}$$

with α the optical absorption coefficient at the pump beam wavelength. This field is usually one order below the built-in field discussed above so that it is necessary to perform experiment at a very low level of pump laser fluence. In Fig. 12(c), the inverse piezoelectric effect is evidenced in non-doped (10^8 cm^{-3}) GaAs A[1 1 1] sample. At low fluence, the piezoelectric signal is in antiphase to the high fluence signal which is governed by the deformation potential because of the saturation of the photoinduced

Dember electric field [88]. That dephasing arises from the fact that photoinduced deformation potential stress is always negative for Brillouin zone center photoexcitation, while for face A, the photoinduced inverse piezoelectric stress is positive. This different sign is well evidenced by the occurrence of a competing phenomena leading to vanishing Brillouin signal at a given pump fluence ($0.67\ \mu J\ cm^{-2}$). It is worth mentioning that photo-induced Dember field can also cause the generation of the optical phonons as already ben reported in semiconductors [89].

In the above experimental illustrations, the analysis of the magnitude of photoinduced CAP is important to reveal the characteristic signature of non-linear behavior of the inverse piezoelectric effect. Generally, the detailed analysis also provides rich information on the microscopic processes. Recent picosecond interferometry experiments in n-doped [28] and non-doped [86] GaAs have indeed demonstrated the high sensitivity of the phase of the photo-generated acoustic signal at Brillouin frequency, i.e., the phase of the so-called Brillouin oscillation, to the characteristic time of the photo-induced stress development. In particular, in the experiments with red pump of n-doped GaAs [28] the non-equilibrium electrons and holes are photo-generated in the near surface region, which is much deeper than the charge depletion zone. In this situation, experimentally observed phase delay in the Brillouin oscillation is caused by a finite time of charge carriers diffusion from the photo-excited volume to the near-surface depletion zone, where they are spatially separating by the built-in field and are screening this built-in electric field. In the non-doped GaAs photo-excited by blue pump radiation, which penetrates just about 15 nm in the sample, the phase delay in the detected Brillouin oscillations is related to the Maxwell relaxation time of photo-excited charge carriers [86]. In non-doped GaAs the built-in electric field is absent. The Maxwell relaxation time is the time for the spatial separation of the locally photo-excited electrons and holes, caused by higher diffusivity of the electrons in comparison with that of the holes. At the time scale of Maxwell relaxation, fast diffusion of the electrons from the photo-excited surface of the semiconductor becomes completely compensated by their drift towards the surface in the field of the holes localized in the photo-excitation region. Thus, after femtosecond laser excitation of non-doped GaAs by blue light, the electric field, which is due to the spatial separation of electrons and holes and which generates sound through the inverse PE effect, is developed with a temporal delay equal to the Maxwell relaxation time [86].

As a concluding illustration, it is worth to mention that CAP generation by inverse piezoelectric effect can be also achieved in ferroelectric materials that are known to exhibit superior piezoelectric properties compared to semiconductors. These studies are recent and are still the subject of active discussions. Among the recent works, a UV pump/X-ray probe experiment was performed on the canonical ferroelectric $PbTiO_3$. It has been reported a light-induced modification of the tetragonality that has been explained by a modulation of the internal electric field pre-existing in the ferroelectric film driven by the photoexcited carriers [39]. Moreover, the piezoelectric signature has been confirmed by the observation of a saturation of the $PbTiO_3$ lattice parameter when light excitation intensity increases up to a full screening of the internal electric field. This latter effect is consistent with what was already observed in piezoelectric semiconductor GaAs [27] (see Fig. 11(b)). Furthermore, several experiments performed on the room temperature ferroelectric $BiFeO_3$ (BFO) suggest an important contribution of the inverse piezo-electric effect too [38,40,41]. In particular, it has been reported recently that the photo-generation/photo-detection processes of transverse acoustic modes are very efficient in polycrystalline ferroelectric $BiFeO_3$. This spectacular effect, that can be controlled according to the BFO grain orientation, has been attributed to an efficient inverse piezoelectric mechanism [41].

3.4. Electrostriction

3.4.1. Principle of electrostriction

When a medium is transparent (no absorption of light) the photoinduced stress that takes place is due to electrostriction mechanism. This effect is allowed for any point group of symmetry. The local light electric field of the incident pump laser beam can polarize the medium which induces a deformation of the orbitals. This can be even viewed as a centrosymmetry breaking induced by the light electric field which in turn leads to a second order piezoelectric effect. That is the reason why electrostriction can be considered as second order phenomenon according to the electric field E, while piezoelectric effect (non zero first order piezoelectric tensor) is a first order phenomenon.

If the orbitals are distorted, the electrons distribution and orbitals overlapping are modified and this leads to both modifications of the density ρ and the dielectric constant ϵ that can be linked by:

$$\Delta\epsilon = \frac{\partial\epsilon}{\partial\rho}\Delta\rho \tag{23}$$

The modification of the dielectric constant ($\Delta\epsilon$) leads to a modification of the electromagnetic density of energy with:

$$\Delta w = \frac{1}{2}\Delta\epsilon E^2 = \frac{1}{2}\frac{\partial\epsilon}{\partial\rho}\Delta\rho E^2 \tag{24}$$

According to the first principle of thermodynamics law, the variation of this energy is associated to a work ($\Delta w = -P\Delta V/V$) provided by the material. With $\Delta\rho/\rho = -\Delta V/V$, the corresponding electrostriction stress becomes then:

$$\sigma_{ES} = -\frac{1}{2}\rho\frac{\partial\epsilon}{\partial\rho}E^2 \tag{25}$$

The term $\rho\frac{\partial\epsilon}{\partial\rho}$ is called the electrostrictive parameter.

Different formulations can be obtained [30–32,51] and in the general case it is necessary to account for tensorial nature of each of the physical mechanisms contributing to ES stress [30]:

$$(\sigma_{ES})_{ji} = \frac{1}{8\pi}P_{klji}\epsilon_{km}\epsilon_{ln}E_mE_n \tag{26}$$

where P_{klji}, ϵ_{km} and E_m are the photoelastic tensor, it is worth to note that electrostriction phenomenon depends on the polarization of the incident electric field, so that either longitudinal or transverse acoustic phonons can be photogenerated. The dielectric constant and the pump light pulse electric field.

3.4.2. Experimental observations

Only few experimental evidences of sound generation through ES mechanism finally exist and most of them are based on the application of the transient optical-gratings method [31,32]. This method consists in using two oblique pump laser beams to induce an optical interference in the plane of the irradiated surface. By this way, the different angle (wave vector of the incident beams) between two pump beam permits to choose a given periodicity of the grating, this means to select a given wavelength of the emitted acoustic wave and hence a given acoustic frequency. One example is given in Fig. 13 where longitudinal coherent acoustic phonons have been photoexcitated by the transient gratings methods in liquid carbon disulfide. In this study, a phase-sensitive heterodyne method for the detection has been employed which allows to record not only the amplitude of coherent density oscillations but also the phase. Then, the expected behavior of a complex resonance spectrum of a forced oscillator is evidenced in Fig. 13. More recently electrostriction (called photostriction) has

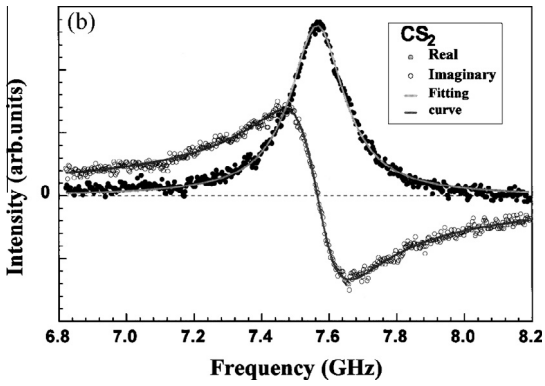

Fig. 13. Photogeneration of acoustic waves by electrostriction and using a transient gratings method in CS_2 [32], the figure represents the complex anti-stoke Brillouin signal (real and imaginary part) at room temperature where we recognize the typical complex spectrum of a forced oscillator. Copyright (1997) by The American Physical Society.

been proposed as a possible contributing mechanism of photogeneration of CAP in multiferroic compound $BiFeO_3$ [90] even if the mechanism of light-induced strain remains debated in these complex oxides family [26,39,41]. Promising issues are expected with the ES mechanism, since some theoretical estimates have shown that ES mechanism, initiated by an ultrashort laser pulse crossing the interface between two transparent media, could lead to the excitation of the compression/dilatation and shear acoustic pulses with the duration controlled by the duration of the laser pulse [30]. However, no observation of such possibilities has been reported yet.

4. Summary and current opened questions

It is of course impossible to give a complete and detailed overview of these rich physical processes that take place within the solids submitted to femtosecond light pulse within few pages. This is then only an attempt of updating of the new achievements of ultrafast acoustics community. Even if advanced understanding of the microscopic mechanisms for so-called conventional systems like metals or semiconductors has been achieved, there are still rich phenomena that require further investigations like CAP photogeneration in cooperative systems exhibiting charge, spin ordering, like the ferroelectrics or multiferroics materials. Unusual phenomena related to photoinduced strain can be expected as already reported in charge-ordering and Metal–Insulator oxides [34,37,91] where clear non-thermal contribution has been evidenced. The recent experiments on ferroelectric materials, exhibiting very large internal polarization as well as large piezoelectric constant, have given rise to numerous discussions on the microscopic mechanisms involved after the action of femtosecond laser pulses and in particular about the coherent lattice response in the excited ferroelectric domains [26,35,36,38,39,92]. As a coherent acoustic phonons wavepacket connects, from the elastic point of view, several unit cells, as a matter of fact, the photoinduced strain field should indeed provide information on the cooperativity in phase-transition systems but this approach has been only poorly investigated up to now. Recent photoinduced phase transitions observations report some peculiar role of the acoustic phonons. Some macroscopic phase transformations, initiated at the free surface by a femtosecond light pulse, appear to develop from the surface towards the bulk at the speed of sound [93].

Acknowledgements

We would like to thank our colleagues from Le Mans, G. Vaudel, V. Temnov, T. Pezeril, N. Chigarev and many colleagues from the ultrafast acoustics community, B. Perrin, B. Jusserand, A. Huynh, E. Peronne, D. Lanzillotti-Kimura, O. Wright, O. Matsuda, C-K Sun, T. Dekorsy, A. Akimov, A. Kent and H. J. Maris for the many active and friendly discussions we had the past decade. We would like also to thank B. Dkhil and I. C. Infante for fruitful discussions on ferroelectrics.

References

[1] C. Thomsen, J. Strait, Z. Vardeny, H.J. Maris, J. Tauc, J.J. Hauser, Coherent phonon generation and detection by picosecond light pulses, Phys. Rev. Lett. 53 (1984) 989.
[2] G.L. Eesley, B.M. Clemens, C.A. Paddock, Generation and detection of picosecond acoustic pulses in thin metal films, Appl. Phys. Lett. 50 (1987) 717.
[3] C. Thomsen, H.T. Grahn, H.J. Maris, J. Tauc, Surface generation and detection of phonons by picosecond light pulses, Phys. Rev. B 34 (1986) 4129.
[4] V. Gusev, A. Karabutov, Laser Optoacoustics, AIP, New York, 1993.
[5] T. Saito, O. Matsuda, O.B. Wright, Picosecond acoustic phonon pulse generation in nickel and chromium, Phys. Rev. B 67 (2003) 205421.
[6] G. Tas, H.J. Maris, Electron diffusion in metals studied by picosecond ultrasonics, Phys. Rev. B 49 (1994) 15046.
[7] O.B. Wright, V.E. Gusev, Ultrafast acoustic phonon generation in gold, Physica B 219-220 (1996) 770–772.
[8] O.B. Wright, Ultrafast non-equilibrium stress generation in gold and silver, Phys. Rev. B 49 (1994) 9985.
[9] O.B. Wright, V. Gusev, Ultrafast generation of acoustic waves in copper, IEEE UFFC 42 (1995) 331.
[10] M. Lejman, V. Shalagatskyi, O. Kovalenko, T. Pezeril, V.V. Temnov, P. Ruello, Ultrafast optical detection of coherent acoustic phonons emission driven by superdiffusive hot electrons, J. Opt. Soc. Am. B 31 (2014) 282–290.
[11] O.B. Wright, B. Perrin, O. Matsuda, V.E. Gusev, Ultrafast carrier diffusion in gallium arsenide probed with picosecond acoustic pulses, Phys. Rev. B 64 (2001) 081202.
[12] P. Babilotte, P. Ruello, D. Mounier, T. Pezeril, G. Vaudel, M. Edely, J-M. Breteau, V. Gusev, K. Blary, Femtosecond laser generation and detection of high-frequency acoustic phonons in GaAs semiconductors, Phys. Rev. B. 81 (2010) 245207.
[13] E.S.K. Young, A.V. Akimov, R.P. Campion, A.J. Kent, V. Gusev, Picosecond strain pulses generated by a supersonically expanding electron-hole plasma in GaAs, Phys. Rev. B 86 (2013) 155207.
[14] A. Bartels, T. Dekorsy, H. Kurz, K. Khler, Coherent zone-folded longitudinal acoustic phonons in semiconductor superlattices: excitation and detection, Phys. Rev. Lett. 82 (1999) 1044.
[15] A. Huynh, B. Perrin, N.D. Lanzillotti-Kimura, B. Jusserand, Fainstein A, A. Lemaitre, Subterahertz monochromatic acoustic wave propagation using semiconductor superlattices as transducers, Phys. Rev. B. 78 (2008) 233302.
[16] C-K. Sun, J-C. Liang, X-Y. Yu, Coherent acoustic phonon oscillations in semiconductor multiple quantum wells with piezoelectric fields, Phys. Rev. Lett. 84 (2000) 179.
[17] M.F. Pascual-Winter, A. Fainstein, B. Jusserand, B. Perrin, A. Lematre, Spectral responses of phonon optical generation and detection in superlattices, Phys. Rev. B 85 (2012) 235443.
[18] J.J. Baumberg, D.A. Williams, K. Köhler, Ultrafast acoustic phonon ballistics in semiconductor heterostructures, Phys. Rev. Lett. 78 (1997) 3358.
[19] O. Matsuda, T. Tachizaki, T. Fukui, J.J. Baumberg, O.B. Wright, Acoustic phonon generation and detection in GaAs/Al0.3Ga0.7As quantum wells with picosecond laser pulses, Phys. Rev. B. 71 (2005) 115330.
[20] P.-A. Mante, A. Devos, A. Le Louarn, Generation of terahertz acoustic waves in semiconductor quantum dots using femtosecond laser pulses, Phys. Rev. B 81 (2008) 113305.
[21] E. Peronne, E. Charron, S. Vincent, S. Sauvage, A. Lemaitre, B. Perrin, B. Jusserand, Two-color femtosecond strobe lighting of coherent acoustic phonons emitted by quantum dots, Appl. Phys. Lett. 102 (2013) 043107.
[22] O. Matsuda, O.B. Wright, D.H. Hurley, V.E. Gusev, Coherent shear phonon generation and detection with ultrashort optical pulses and K. Shimizu, Phys. Rev. Lett. 93 (2004) 095501.
[23] T. Pezeril, P. Ruello, S. Gougeon, N. Chigarev, D. Mounier, J.-M. Breteau, P. Picart, V. Gusev, Generation and detection of plane coherent shear picosecond acoustic pulses by lasers: experiment and theory, Phys. Rev. B 75 (2007) 174307.
[24] T. Pezeril, F. Leon, D. Chateigner, S. Kooi, Keith A. Nelson, Picosecond photoexcitation of acoustic waves in locally canted gold films, Appl. Phys. Lett. 92 (2008) 061908.
[25] Y-C. Wen, T-S. Ko, T-C. Lu, H-C. Kuo, J-I. Chyi, C-K. Sun, Photogeneration of coherent shear phonons in orientated wurtzite semiconductors by piezoelectric coupling, Phys. Rev. B 80 (2009) 195201.

[26] P. Ruello, T. Pezeril, S. Avanesyan, G. Vaudel, V. Gusev, I.C. Infante, B. Dkhil, Photoexcitation of gigahertz longitudinal and shear acoustic waves in $BiFeO_3$ multiferroic single crystal, Appl. Phys. Lett. 100 (2012) 212906.

[27] P. Babilotte, P. Ruello, G. Vaudel, T. Pezeril, D. Mounier, J-M. Breteau, V. Gusev, Picosecond acoustics in p-doped piezoelectric semiconductors, Appl. Phys. Lett. 97 (2010) 174103.

[28] P. Babilotte, P. Ruello, T. Pezeril, G. Vaudel, D. Mounier, J.-M. Breteau, V. Gusev, Transition from piezoelectrical generation of hypersound to its generation by deformation potential mechanism with increasing fluence of ultrafast laser action on GaAs, J. Appl. Phys. 109 (2011) 064909.

[29] K-H. Lin, C-T. Yu, Y-C. Wen, C-K. Sun, Generation of picosecond acoustic pulses using a p–n junction with piezoelectric effects, Appl. Phys. Lett. 86 (2005) 093110.

[30] V. Gusev, P. Picart, D. Mounier, J.-M. Breteau, On the possibility of ultrashort shear acoustic pulse excitation due to the laser-induced electrostrictive effect, Opt. Comm. 204 (2002) 229–236.

[31] Y-X. Yan, E.B. Gamble, K.A. Nelson, Impulsive stimulated scattering: General importance in femtosecond laser pulse interactions with matter, and spectroscopic applications, J. Chem. Phys. 83 (1985) 5392.

[32] H. Tanaka, T. Sonehara, S. Takagi, A new phase-coherent light scattering method: first observation of complex Brillouin spectra, Phys. Rev. Lett. 79 (1997) 881.

[33] W. Maryam, A.V. Akimov, R.P. Campion, A.J. Kent, Dynamics of a vertical cavity quantum cascade phonon laser structure, Nature Commun. 4 (2013) 2184.

[34] D. Lim, V.K. Thorsmolle, R.D. Averitt, Q.X. Jia, K.H. Ahn, M.J. Graf, S.A. Trugman, A.J. Taylor, Coherent optical and acoustic phonon generation correlated with the charge-ordering phase transition in $La_{1-x}Ca_xMnO_3$, Phys. Rev. B 71 (2005) 134403.

[35] C.v. Korff Schmising, A. Harpoeth, N. Zhavoronkov, Z. Ansari, C. Aku-Leh, M. Woerner, T. Elsaesser, M. Bargheer, M. Schmidbauer, I. Vrejoiu, D. Hesse, M. Alexe, Phys. Rev. B 78 (2008) 060404.

[36] C.v. Korff Schmising, M. Bargheer, M. Kiel, N. Zhavoronkov, M. Woerner, T. Elsaesser, I. Vrejoiu, D. Hesse, M. Alexe, Phys. Rev. Lett. 98 (2007) 257601.

[37] P. Ruello, S. Zhang, P. Laffez, B. Perrin, V. Gusev, Laser-induced coherent acoustic phonon mechanisms in Metal–Insulator compounds $NdNiO_3$: thermal and non-thermal processes, Phys. Rev. B 79 (2009) 094303.

[38] H. Wen, P. Chen, M.P. Cosgriff, D.A. Walko, J.H. Lee, C. Adamo, R.D. Schaller, J.F. Ihlefeld, E.M. Dufresne, D.G. Schlom, P.G. Evans, J.W. Freeland, Y. Li, Electronic origin of ultrafast photoinduced strain in $BiFeO_3$, Phys. Rev. Lett 110 (2013) 037601.

[39] D. Daranciang, M.J. Highland, H. Wen, S.M. Young, N.C. Brandt, H.Y. Hwang, M. Vattilana, M. Nicoul, F. Quirin, J. Goodfellow, T. Qi, I. Grinberg, D.M. Fritz, M. Cammarata, D. Zhu, H.T. Lemke, D.A. Walko, E.M. Dufresne, Y. Li, J. Larsson, D.A. Reis, K. Sokolowski-Tinten, K.A. Nelson, A.M. Rappe, P.H. Fuoss, G.B. Stephenson, A.M. Lindenberg, Ultrafast photovoltaic response in ferroelectric nanolayers, Phys. Rev. Lett 110 (2013) 037601.

[40] D. Schick, M. Herzog, H. Wen, P. Chen, C. Adamo, P. Gaal, D.G. Schlom, P.G. Evans, Y. Li, M. Bargheer, Localized excited charge carriers generate ultrafast inhomogeneous strain in the multiferroic $BiFeO_3$, Phys. Rev. Lett. 112 (2014) 097602.

[41] M. Lejman, G. Vaudel, I-C. Infante, P. Femeiner, V. Gusev, B. Dkhil, P. Ruello, Giant Ultrafast photoinduced shear strain in ferroelectroc $BiFeO_3$, Nature Commun. 5 (2014) 4301.

[42] A. Devos, C. Lerouge, Evidence of laser-wavelength effect in picosecond ultrasonics: possible connection with interband transitions, Phys. Rev. Lett. 86 (2003) 2669.

[43] B. Perrin, B. Bonello, J.C. Jeannet, E. Romanet, Interferometric detection of hypersound waves in modulated structures, Prog. Nat. Sci. 6 (1996) 444.

[44] B. Perrin, C. Rossignol, B. Bonello, J-C. Jeannet, Interferometric detection in picosecond ultrasonics, Physica B 263-64 (1999) 863.

[45] O. Matsuda, M. Tomoda, T. Tachizaki, S. Koiwa, A. Ono, K. Aoki, R.P. Beardsley, O.B. Wright, Ultrafast ellipsometric interferometry for direct detection of coherent phonon strain pulse profiles, J. Opt. Soc. Am. B 30 (2013) 1911.

[46] N. Chigarev, C. Rossignol, B. Audoin, Surface displacement measured by beam distortion detection technique: application to picosecond ultrasonics, Rev. Sci. Instrum. 77 (2006) 114901.

[47] H. Cailleau, M. Lorenc, L. Guérin, M. Servol, E. Collet, M. Buron-Le, Cointe Structural dynamics of photoinduced molecular switching in the solid state, Acta Cryst. A. 66 (2010) 189–197.

[48] A.C. Tam, Applications of photoacoustic sensing techniques, Rev. Mod. Phys. 58 (1986) 381–431.

[49] P. Yu, M. Cardona, Fundamentals of Semiconductors, Springer Verlag, Heidelberg, 1998.

[50] T. Kohmoto, K. Tada, T. Moriyasu, Y. Fukuda, Observation of coherent phonons in strontium titanate: structural phase transition and ultrafast dynamics of the soft modes, Phys. Rev. B. 74 (2006) 064303.

[51] R. Merlin, Generating coherent THz phonons with light pulses, Sol. State. Com. 102 (1997) 207–220.

[52] S.A. Akhmanov, V.E. Gusev, Sov. Phys. Usp. 35 (3) (1992) 153.

[53] V. Gusev, Laser hypersonics in fundamental and applied research, ACUSTICA – Acta Acust. 82 (1996) S37–S45.

[54] M. Perner, S. Gresillon, J. Mrz, G. von Plessen, J.FeldmannJ. Porstendorfer, K.-J. Berg, G. Berg, Observation of hot-electron pressure in the vibration dynamics of metal nanoparticles, Phys. Rev. Lett. 85 (2000) 792.

[55] N.W. Aschroft, N.D. Mermin, Solid State Physics, Saunders College Publishing, Orlando, 1976.

[56] E.M. Lifshitz, L.P. Pitaevskii, Physical Kinetics, Course on Theoretical Physics, vol. 10, Pergamon, Oxford, 1981.

[57] M.I. Kaganov, I.M. Lifshitz, I.V. Tantarov, Relaxation between electrons and lattice, Sov. Phys. JETP 4 (1957) 173.

[58] G.L. Eesley, Generation of nonequilibrium electron and lattice temperatures in copper by picosecond laser pulses, Phys. Rev. B 33 (1986) 2144.

[59] P.B. Allen, Theory of thermal relaxation of electrons in metals, Phys. Rev. Lett. 59 (1987) 1460.

[60] V.E. Gusev, O.B. Wright, Ultrafast nonequilibrium dynamics of electrons in metals, Phys. Rev. B 57 (1998) 2878.

[61] V.E. Gusev, On the duration of acoustic pulses excited by subpicosecond laser action on metals, Opt. Comm. 94 (1992) 76–78.

[62] C. Voisin, N. Del Fatti, D. Christofilos, F. Vallé, Time-resolved investigation of the vibrational dynamics of metal nanoparticles, Appl. Surf. Sci. 164 (2000) 131.

[63] Wang J. Gui C, Effect of electron heating on femtosecond laser-induced coherent acoustic phonons in noble metals, Phys. Rev. B 75 (2007) 184304.

[64] S. Adachi, GaAs and Related Materials (Bulk Semiconductors and Superlattice Properties), World Scientific, Singapore, 1994.

[65] O.B. Wright, V.E. Gusev, Acoustic generation in crystalline silicon with femtosecond optical pulses, Appl. Phys. Lett. 66 (1995) 1190.

[66] P. Babilotte, E. Morozov, P. Ruello, D. Mounier, M. Edely, J-M. Breteau, A. Bulou, V. Gusev, Physical mechanism of coherent acoustic phonons generation and detection in GaAs semiconductor, J. Phys.: Conf. Ser. 92 (2007) 012019.

[67] D. Yu. Paraschuk, N. Chigarev, X.Y. Pan, V. Gusev, Coherent acoustic emission in the supersonic expansion of the photogenerated electron-hole plasma, Phys. Rev. B 61 (2000) 15837–15840.

[68] V.E. Gusev, Generation of picosecond acoustic pulses by laser radiation in piezosemiconductors, Phys. Stat. Sol. (b) 158 (1990) 367–381.

[69] N. Chigarev, D. Yu. Paraschuk, X.Y. Pan, V. Gusev, Laser hyperacoustic spectroscopy of single Crystal germanium, Sov. Phys.: J. Exp. Theor. Phys. (JETP) 94 (2002) 627–636.

[70] S. Avanesyan, V. Gusev, N. Zheludev, Generation of deformation waves in the process of photoexcitation and recombination of nonequilibrium carriers in silicon, Appl. Phys. A 40 (1986) 163–166.

[71] E.S. Harmon, M.R. Melloch, J.M. Woodall, D. D Nolte, N. Otsuka, C.L. Chang, Carrier lifetime versus anneal in low temperature growth GaAs, App. Phys. Lett. 63 (1993).

[72] E. Morosoz, P. Ruello, V. Gusev, unpublished.

[73] H.J. Maris, in: W.P. Mason, R.N. Thurston (Eds.), Physical Acoustics, vol. 7, Academic, New York, 1971, p. 279.

[74] S.D. Brorson, A. Kazeroonian, J.S. Moodera, D.W. Face, T.K. Cheng, E.P. Ippen, M.S. Dresselhaus, G. Dresselhaus, Femtosecond room-temperature measurement of the electron–phonon coupling constant λ in metallic superconductors, Phys. Rev. Lett. 64 (1990) 2172.

[75] K.J. Manke, A.A. Maznev, C. Klieber, V. Shalagatskyi, V.V. Temnov, D. Makarov, S.-H. Baek, C.-B. Eom, K.A. Nelson, Measurement of shorter-than-skin-depth acoustic pulses in a metal film via transient reflectivity, Appl. Phys. Lett. 103 (2013) 173104.

[76] T. Pezeril, C. Klieber, S. Andrieu, K.A. Nelson, Optical generation of gigahertz-frequency shear acoustic waves in liquid glycerol, Phys. Rev. Lett. 102 (2009) 107402.

[77] C. Rossignol, J-M. Rampnoux, M. Perton, B. Audoin, S. Dilhaire, Phys. Rev. Lett. 94 (2005) 166106.

[78] D.H. Hurley, O.B.Wright O. Matsuda, V.E. Gusev, O.V. Kolosov, Laser picosecond acoustics in isotropic and anisotropic materials, Ultrasonics 38 (2000) 470–474.

[79] T. Bienville, B. Perrin, in: Proceedings of WCU, 2003, unpublished, p. 813. <sfa.asso.fr/wcu2003/procs/website/>.

[80] J.F. Nye, Physical Properties of Crystals: Their Representation by Tensors and Matrices, Oxford University Press, 1985. p. 329.

[81] Karin M. Rabe, Charles H. Ahn, Jean-Marc Triscone (Eds.) Physics of Ferroelectrics, A Modern Perspective Series: Topics in Applied Physics, vol. 105(XII), 2007, p. 388.

[82] S.M. Sze, Physics of Semiconductors Devices, John Wiley&Sons, New York, 1981.

[83] K-H. Lin, C-T. Yu, Y-C. Wen, C-K. Sun, Generation of picosecond acoustic pulses using a p–n junction with piezoelectric effects, Appl. Phys. Lett. 86 (2005) 093110.

[84] C-C. Chen, H-M. Huang, T-C. Lu, H-C. Kuo, C-K Sun, Magnitude-tunable sub-THz shear phonons in a non-polar GaN, multiple-quantum-well p-i-n diode, Appl. Phys. Lett. 100 (2012) 201905.

[85] C.S. Kim, J.H. Kim, H. Jeong, Y.D. Jho, H.K. Kwon, H.S. Lee, J.S. Park, K. Song, S.H. Kim, Y.J. Kim, D. Lee, K.J. Yee, Control of coherent acoustic phonon generation with external bias in InGaN/GaN multiple quantum wells, Appl. Phys. Lett. 100 (2012) 101105.

[86] G. Vaudel, P. Ruello, T. Pezeril, V. Gusev, Competition between inverse piezoelectric effect and deformation potential mechanism in undoped GaAs revealed by ultrafast acoustics, Eur. Phys. J. 41 (2013) 04005.

[87] G. Vaudel, T. Pezeril, A. Lomonosov, M. Lejman, P. Ruello, V. Gusev, Generation of hypersound by photo-Dember electric field. Phys. Rev. B 2014, in press.

[88] H. Dember, Photoelectric E.M.F. in cuprous-oxide crystals, Phyz. Z. 32 (1931) 554.

[89] T. Dekorsy, H. Auer, C. Waschke, H.J. Bakker, H.G. Roskos, H. Kurz, V. Wagner, P. Grosse, Emission of submillimeter electromagnetic waves by coherent phonons, Phys. Rev. Lett. 74 (1995) 738.
[90] L.Y. Chen, J.C. Yang, C.W. Luo, C.W. Laing, K.H. Wu, J.-Y. Lin, T.M. Uen, J.Y. Juang, Y.H. Chu, T. Kobayashi, Ultrafast photoinduced mechanical strain in epitaxial $BiFeO_3$ thin films, App. Phys. Lett. 101 (2012).
[91] P. Ruello, S. Zhang, P. Laffez, B. Perrin, V. Gusev, Ultrafast electronic dynamics in the metal-insulator transition compound $NdNiO_3$, Phys. Rev. B 76 (2007) 165107.
[92] K-J. Jang, H-G Lee, S. Lee, J. Ahn, J.S. Ahn, N. Hur, S-W. Cheong, Strong spin-lattice coupling in multiferroic hexagonal manganite $YMnO_3$ probed by ultrafast optical spectroscopy, Appl. Phys. Lett. 97 (2010) 031914.
[93] M. Lorenc, Ch. Balde, W. Kaszub, A. Tissot, N. Moisan, M. Servol, M. Buron-Le Cointe, H. Cailleau, P. Chasle, P. Czarnecki, M.L. Boillot, E. Collet, Cascading photoinduced, elastic, and thermal switching of spin states triggered by a femtosecond laser pulse in an Fe(III) molecular crystal, Phys. Rev. B 85 (2012) 054302.